

GT2011-46333

HEAT TRANSFER IN A CHANNEL UNDER EFFECTS OF A SHALLOW-ANGLE JET IMPINGEMENT AND A RIB

Lei Wang
Lund University
Lund, 22100, Sweden

Bengt Sundén
Lund University
Lund, 22100, Sweden

Andreas Borg
Volvo Aero Corporation
Trollhättan, 46181, Sweden

Hans Abrahamsson
Volvo Aero Corporation
Trollhättan, 46181, Sweden

ABSTRACT

Experimental studies are carried out to investigate the heat transfer characteristics involving an impinging jet with a shallow-angle in a crossflow. A rib is applied to control the jet impingement heat transfer. Liquid crystal technique is employed to measure the wall temperature and obtain the heat transfer coefficients. In the study, the Reynolds number for the crossflow is 80,000 and the Reynolds number for the jet ranges from 20,000 to 40,000. This gives rise to the jet-to-crossflow velocity ratio varying from 1.4 to 2.8. For all the tested cases, it is found that the presence of rib makes the Nusselt number profiles across the stagnation point change from a classical bell-shaped profile to a plateau-like pattern, indicating the enhanced heat transfer region expands more as the rib is present. In particular, the presence of rib has a more pronounced effect on the enhancement of heat transfer at lower velocity ratio ($R = 1.4$). However, in such case, the local heat transfer in the rib corner region deteriorates. At higher velocity ratio, especially at $R = 2.8$, the presence of rib makes the heat transfer rate more uniform, but meanwhile, it is found that the impinging jet effect tends to be weaker.

INTRODUCTION

Due to its high heat transfer rate, jet impingement has been used in a variety of industrial fields such as cooling of electronic components and drying of paper and textiles. It has been recognized that jet impingement could be an excellent candidate for enhancing gas turbine heat transfer. In many actual applications of jet impingement, crossflow often exists

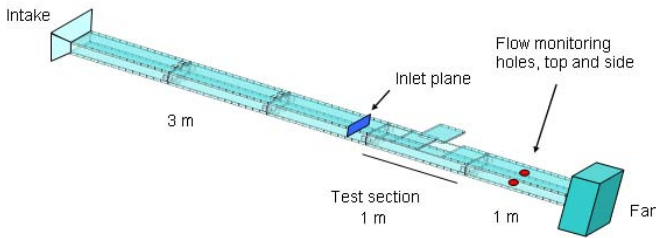
which occurs as the result of the confluence of the upstream jet mass flow in the internal passages. In such case, the stagnation point is shifted downstream and the peak Nusselt number is decreased significantly. The heat transfer characteristics of jet impingement in crossflow have been reported in [1-5]. However, the jet impingement has a disadvantage that the heat transfer deteriorates rapidly outside the jet impingement region. The non-uniform heat transfer can cause thermal stresses which have a potential risk for the operational safety of, for instance, gas turbines. To counteract the adverse effect, there have been many studies on control of heat transfer characteristics of impinging jet in crossflow. Under the condition of crossflow, Jia et al. [6] showed that the jet array impingement heat transfer was enhanced considerably in a ribbed-roughed channel. Kanokjaruvijit and Martinez-botas [7] investigated the heat transfer characteristics of jet array impingement on a dimpled surface with different crossflow schemes. The flow mechanism of dimple impingement might be considered as a couple effect of jet impingement and channel flow with vortex shedding occurred in the staggered dimple array. Overall speaking, the heat transfer was more enhanced with the maximum crossflow and larger jet-to-plate spacing. They also found that geometries of dimple have limited effects on the performance of heat transfer. Nam et al. [8] studied the heat transfer in impingement/effusion cooling system in crossflow with rib turbulators. The results showed that higher heat transfer rate than that for a surface without ribs because the ribs prevent the wall jets from being swept away by the crossflow and increase local turbulence of the flow near the surface. Yan and Saniei [9] applied liquid crystal technique to measure the local Nusselt number from an obliquely impinging circular air jet to a flat plate. The oblique angles were selected to be 90° , 75° , 60° , and 45° . They showed that for a given situation, the point of the

maximum heat transfer shifts away from the geometrical impingement point towards the compression side of the jet. However, to the knowledge of authors, the effects of very shallow angle in jet impingement on heat transfer, for example, $\theta < 20^\circ$, is not found in public literature.

In this study, we aim to investigate the jet impingement with very shallow impingement angle in a channel crossflow. A rib is applied to control the heat transfer, especially in the stagnation zone. This work is motivated by the internal cooling of hot turbine structures. Liquid crystal technique is employed to measure the local heat transfer coefficients.

EXPERIMENTAL SETUP

The test section consists of a 5-meter long channel, made of Plexiglas, to provide optical path for liquid crystal measurements. The whole channel is divided into three sections, i.e., the inlet section (3 meter long), measurement section (1 meter long) and outlet section (1 meter long). The cross section of the channel is 320×80 mm (the thickness is 20 mm). In the measurement section, four parts are divided for the sake of inserting various wall disturbances and jets easily, as shown in Fig. 1. The air is sucked into the channel by a fan whose maximum power is 3.0 kW. By adjusting the frequencies, the flow rates can be reached as desire. The velocity is measured by a Prandtl tube and is checked by Blasius law as well.



The jets are provided by a compressor system. After passing a filter, a tank (to eliminate the compressing effect), a regulating valve, and a flowmeter, air enters a long straight tube. The tube is made of stainless steel with an internal diameter 22.5 mm (d) and outer diameter 25 mm (D), respectively. The tube has a length of 1030 mm ($46d$) to produce a fully developed flow before the nozzle exit. At the end of the straight tube, a bend tube is attached. The jet exit geometry is such that the bend injection tube is cut 10° with respect to the normal axis. It should be pointed out that such a bend tube generates Dean-type vortices due to the centrifugal force. The counter-rotating longitudinal vortices can promote mixing of the jet shear layer. This is a significant difference from the straight oblique jet. The rib, with cross section of 20 mm (b) by 10 mm (e) where $b/e = 2$, is placed at the end of the first section. The rib obstructs the channel by 12.5% of its height, or, $e/H = 12.5\%$.

The detailed specifications of the jet and the rib are presented in Fig. 2.

The Cartesian coordinates x, y, z are defined in such a way that the x -axis is in the streamwise direction, the y -axis is the wall-normal direction, and z -axis is the spanwise direction. The symmetry plane in the spanwise direction is represented as $z = 0$.

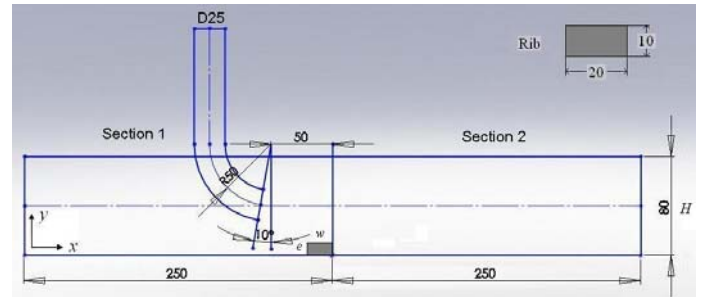


Fig. 2 Specification of jet and rib

The heater is provided by Calesco Foil AB. The resistance wire is made of NiCr alloy. The width of tracks is 1.5 mm and the distance between tracks is 0.2 mm. The uniformity of the heat flux over the heater surface is estimated within 2%. The liquid crystal thermography (LCT) sheet with dimension 250×100 mm is applied on the test section. The configuration of LCT sheet and heating foil is presented in Fig. 3. All the heat transfer measurements are performed in the second section where the thermal boundary layer is believed to be fully developed. This feature will be visited later. Before the execution of experiments, the LCT is calibrated to get the relationship between the temperature and the hue value. LCT images are captured by a GigE Vision CCD camera which allows 1600×1200 pixel resolution. During the experiment, the CCD camera, illumination lighting, and the test section are covered by a dark enclosure to prevent the interference from surrounding light noise. In the present study, the LCT images are captured with spatial resolution of 0.22 mm/pixel. The Cartesian coordinates x, y, z are defined in such a way that the x -axis is in the streamwise direction, the y -axis is the wall-normal direction, and z -axis is the spanwise direction.

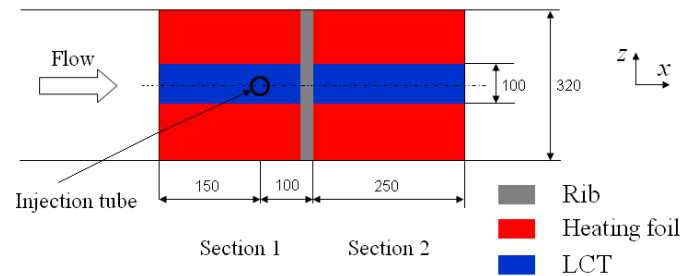


Fig. 3 Configuration of LCT, heating foil and rib arrangement

A liquid crystal technique was employed to measure the heat transfer coefficients on the target plate. After the steady state is achieved, a series of LCT images are generated, each corresponding to a distinct wall heat flux. In interpreting the temperature, the green colour is chosen as the reference colour since it is the most temperature sensitive colour in the calibration curve. The green colour is characterized by the hue value ranging from 60 to 100 (expressed on an 8-bit integer scale) and its resolution is 0.02 °C. By proper adjustment of the wall heat flux, the reference colour is moved from one location to another such that the entire area is eventually covered with the reference colour. This method is essentially based on the principle that the heat transfer coefficient is only a function of the flow conditions and is irrespective of the heating conditions. In the present study, 20-45 LCT images are acquired to extract the local heat transfer coefficients depending on the test conditions.

DATA REJECTION

The Reynolds number for channel flow is defined as $Re_C = U_0 D_h / \nu$, where U_0 is the bulk velocity, and D_h is the hydraulic diameter of the channel. For the fully developed channel flow, the bulk velocity U_0 is determined by measuring the wall static pressure drop. The Reynolds number for jet is defined as $Re_J = U_J d / \nu$, where U_J is the jet exit velocity which is determined by measuring the flow rate, and d is the inner diameter of the injection tube. In addition to the Reynolds number for the jet and crossflow, the jet-to-crossflow velocity ratio, $R = U_J / U_0$, is the most important parameter to scale the flow and heat transfer characteristics.

When calculating the heat transfer coefficient, as stated-above, only points having the hue value within the range from 60 to 100 are processed; outside the selected hue interval, no information is gained. The heat transfer coefficient and Nusselt number based on the hydraulic diameter are defined as $h = \dot{q}_w / (T_w - T_{in})$, where \dot{q}_w is the wall heat flux, T_w and T_{in} are, respectively, the wall temperature and the inlet air temperature. The Nusselt number is defined as $Nu = h D_h / k$, in which k is the thermal conductivity of air. Even though a number of heat fluxes are used, it is found that the maximum air temperature rise from the inlet to the outlet of the channel is less than 2 °C. Therefore, the thermal properties of air are considered to be constant. The Uncertainty analysis is performed by applying the method proposed by Moffat [10]. The uncertainty in local heat transfer coefficients is estimated to be 10% based on the 95% confidence level. This value takes into account the effects of the measuring errors in voltage, current, and LCT reading, the temperature correction for the wall temperature, and the non-uniformity of the heat flux.

RESULTS AND DISCUSSION

1. Preliminary Test

Prior to applying the jet, it is helpful to examine how the thermal boundary layer develops in a smooth channel without jet effect. For $Re_C = 160,000$ for channel flow, Fig. 4 presents the variation of Nusselt number along the centreline (i.e. $z = 0$) of the first test section ($0 \text{ mm} \leq x \leq 250 \text{ mm}$). It is found that the Nusselt number declines quickly and levels off to a plateau as $x > 170 \text{ mm}$. This means that the heat transfer is independent of the streamwise distance as x is greater than 170 mm and the thermal boundary layer after that is fully developed. The dashed line in Fig. 4 indicates the empirical value predicted by the Dittus-Boelter correlation at the same flow conditions. The discrepancy between the two is less than 10%. It should be pointed out that the Nusselt number in the far end region ($x \leq 20 \text{ mm}$) is overestimated due to the edge effect of the heater. In what follows, all the heat transfer measurements will be carried out in the second test section ($250 \text{ mm} \leq x \leq 500 \text{ mm}$).

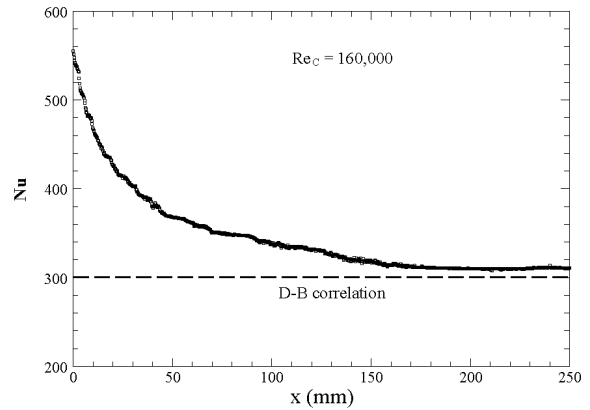


Fig. 4 Thermal boundary layer development in the channel flow

2. Heat Transfer Downstream of Rib without Jet

Before the impinging jet is applied, it is of interest to know the heat transfer pattern downstream of the rib. Figure 5 plots the streamwise variation of the Nusselt number along the centreline, where the streamwise distance x is normalized by the height of the rib. It clearly shows that the heat transfer is considerably enhanced with the increase of the Reynolds number. For each profile, the Nusselt number reaches a maximum value in the vicinity of the location $x/e = 7.5$, which is considered to be the point that the separated shear layer reattaches onto the wall.

Figure 6 presents the variation of the Nusselt number normalized by the smooth channel value Nu_0 at the same Reynolds number. Nu_0 is calculated by means of the Dittus-Boelter correlation. It is clear that the relative enhancement of heat transfer is lower at the higher Reynolds number, which is

consistent with the results of, for example, Wang and Sundén [11] and Kukreja et al. [12].

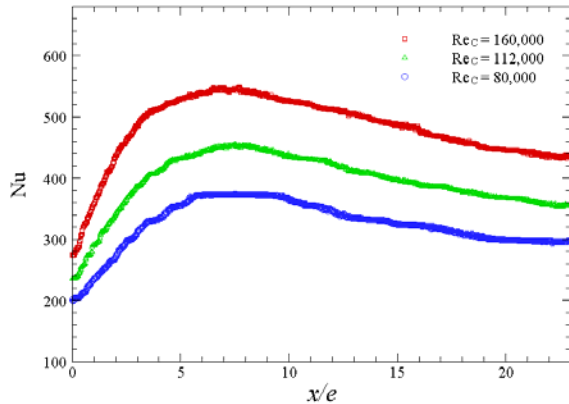


Figure 5 Centerline Nusselt number variation downstream of the rib at different Reynolds numbers

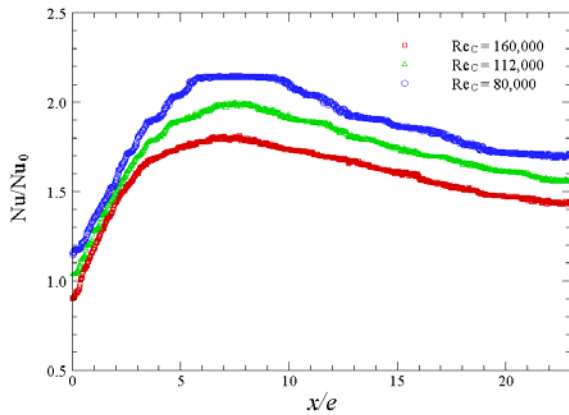


Figure 6 Variation of Nusselt number normalized by Nu_0

Figure 7 demonstrates the variation of the Nusselt number normalized by the respective maximum value at the reattachment point. In the tested Reynolds number range, the different heat transfer profiles collapse well, indicating that the heat transfer downstream of the rib remains similar feature as the Reynolds number varies (Reynolds number similarity). This will greatly simplify the theoretical analysis and lay a foundation for the numerical simulations.

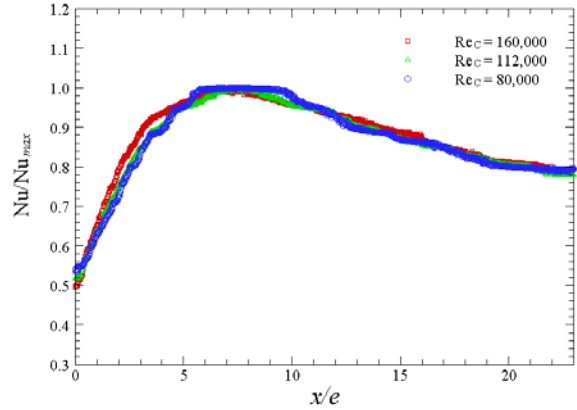


Figure 7 Variation of Nusselt number normalized by Nu_{max}

3. The Effect of Rib on Jet Impingement Heat Transfer in Crossflow

In this section, the emphasis is placed on the rib effect on the impinging jet heat transfer in the channel crossflow. All the measurements are performed at the fixed crossflow Reynolds number, that is, $Re_c = 80,000$. The jet Reynolds numbers vary from 20,000 up to 40,000. This gives rise to the velocity ratio ranging from 1.4 to 2.8. For the sake of easy comparison, the heat transfer characteristics of impinging jet in crossflow without the presence of rib is first presented. Figure 8 demonstrates contour of the local Nusselt number at the velocity ratio $R = 1.4$ (where $Re_j = 20,000$). The distinctive feature is that the jet impinges on the wall directly and a core marked by the highly enhanced heat transfer is formed. Upstream of the core, the Nusselt number is substantially low since the heat transfer is dominated by the crossflow pattern. It should be mentioned that the position of the core (stagnation zone) is, to a large extent, coincident with the reattachment location caused by the rib. Therefore, it is possible to control the jet impingement heat transfer with aid of the rib.

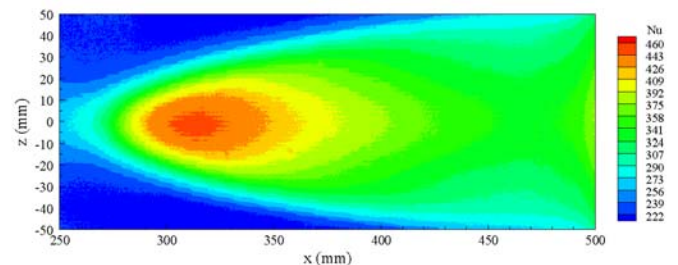


Figure 8 Heat transfer contour at the velocity ratio $R = 1.4$ ($Re_j = 20,000$) in the absence of rib.

Figure 9 presents the contour of local Nusselt number with the effect of rib. Obviously, the heat transfer in the core region is significantly augmented. However, the price is paid to the region just downstream of the rib ($250 \text{ mm} < x < 260 \text{ mm}$)

where the heat transfer is conspicuously deteriorated due to the fact that the fluid velocity in the corner region is very slow and heat is mainly transfer via conduction. This will potentially cause the formation of hot spot and endanger the operational safety of gas turbines.

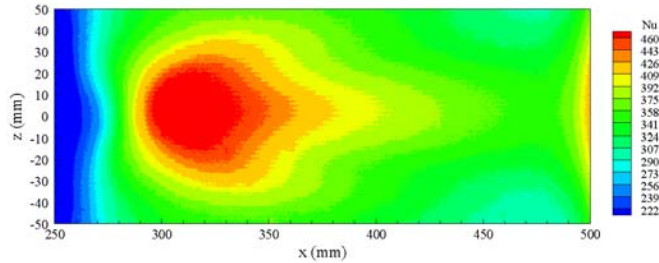


Figure 9 Heat transfer contour at the velocity ratio $R = 1.4$ ($Re_j = 20,000$) in the presence of rib.

Further analysis concerning the effect of rib on jet impingement heat transfer is presented in Fig. 10. In this figure, the point $x_0 = 250$ mm is set as the origin and the streamwise distance is normalized by the internal diameter of the injection tube. It is evident that the heat transfer is intensively enhanced in the stagnation region, but the Nusselt number is low in the region just downstream of the rib compared with the counterpart value without the rib. It is interesting to note that the rib has little impact on the local heat transfer in the wall jet region ($x/d > 5$). It should be pointed out that this conclusion is applied to all the tests in the present study (not shown here).

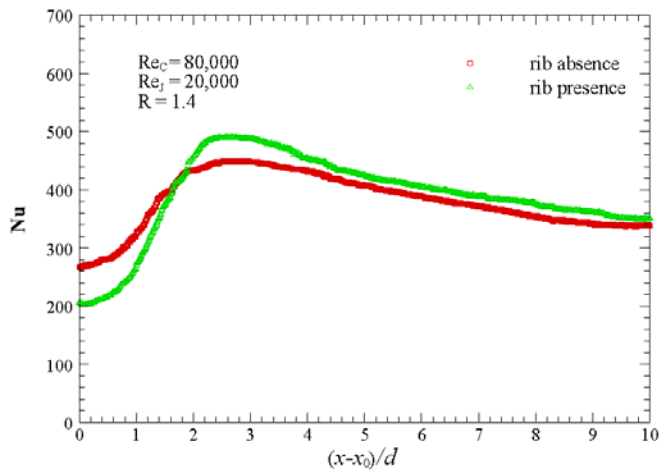


Figure 10 Nusselt number variation along the centerline at $R = 1.4$

Figure 11 displays the Nusselt number across the stagnation point in the spanwise direction. Without the rib, the profile is a bell shape which is characterized by the jet impingement heat transfer; however, due to the presence of the rib, the Nusselt

number distribution becomes a plateau-like pattern, which means that the enhanced region of heat transfer expands more. This will shed a light into the improvement of cooling technique for gas turbines.

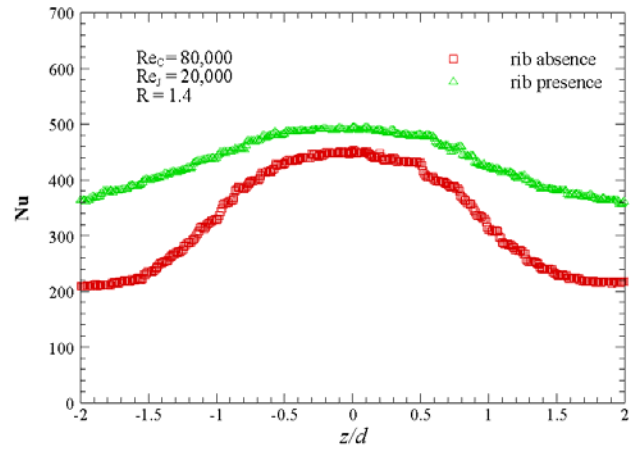


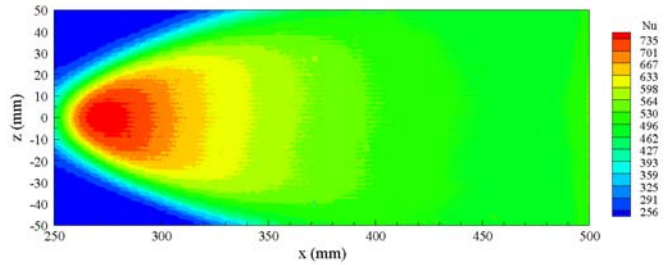
Figure 11 Spanwise Nusselt number variation across the stagnation point at $R = 1.4$ for the rib-absence and rib-presence cases, respectively.

In what follows, we continue to investigate the rib effects on jet impingement heat transfer in crossflow but with different velocity ratios. Figures 12 shows the contours of local Nusselt number at higher velocity ratio $R = 2.0$ for the rib-absence and rib-presence cases. The jet Reynolds numbers $Re_j = 28,000$. Figure 12a shows the local Nusselt number distribution for the rib-absence case. Compared with the contour shown in Fig. 8, it is found that the position of the core shifts upstream since the more powerful jet is less likely to be deflected by the crossflow. Figure 12b gives the contour of Nusselt number with the presence of rib. It is found that the core shape is changed and especially expands in the spanwise direction. The lower heat transfer region just surrounding the core is significantly shrunk.

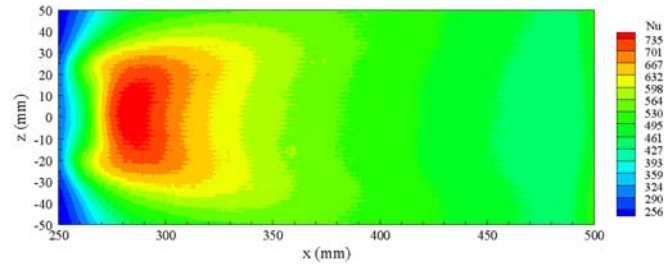
Figure 13 shows the Nusselt number profiles across the stagnation point at $R = 2.0$ for the rib-absence and rib-presence case, respectively. Similar to Fig. 11, the presence of rib turns the bell-shaped distribution into a plateau-like pattern; moreover, the heat transfer is enhanced across the whole tested span. But no difference is perceived in the peak value of Nusselt number since the two curves osculate with each other at the symmetry line.

Figures 14 show the Nusselt number contours at $R = 2.8$ ($Re_j = 40,000$) for the rib-absence and rib-presence case, respectively. At such a high velocity ratio, the jet is dominant over the crossflow to affect the heat transfer. As the rib is absent, Fig. 14a illustrates that the low heat transfer region is mainly located within a small area in the vicinity of the core. As the rib is present, the low heat transfer region is considerably shrunk, as shown in Fig. 14b. On the other hand,

the uniformity of heat transfer rate is increased due to the presence of the rib.



(a) in the absence of rib



(b) in the presence of rib

Figure 12 Heat transfer contour at the velocity ratio $R = 2.0$ ($Re_j = 28,000$) for (a) in the absence of rib; (b) in the presence of rib.

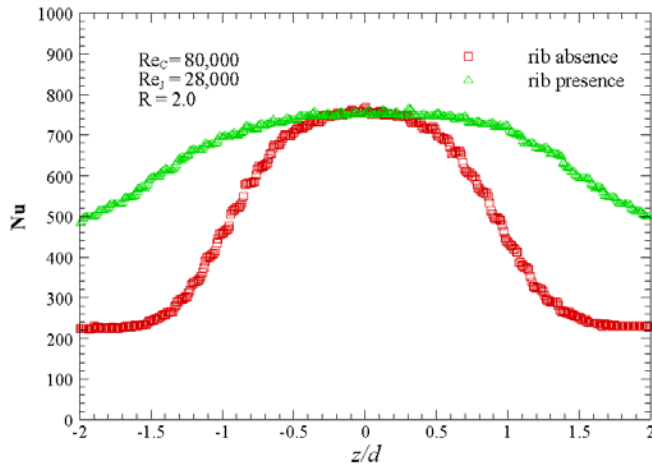
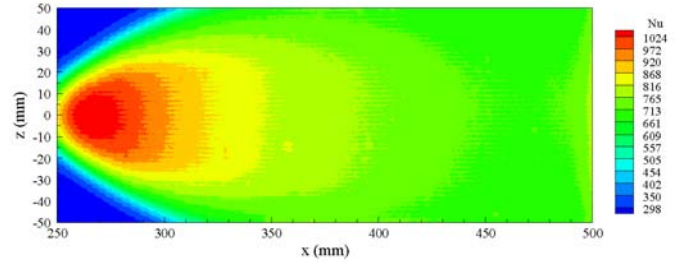


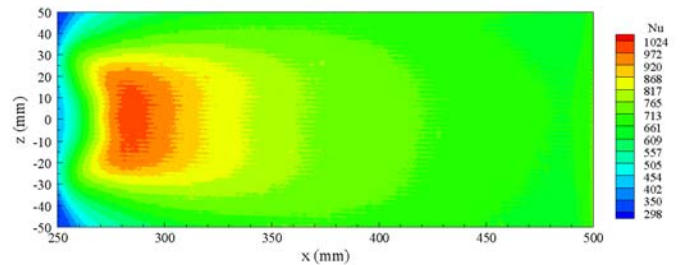
Figure 13 Spanwise variation of Nusselt number across the stagnation point at $R = 2.0$

Figure 15 gives the Nusselt distribution across the stagnation point in the spanwise direction at $R = 2.8$ for the rib-absence and rib-presence cases, respectively. At this velocity ratio, the

two curves intersect and the bell-shaped curve overshoots the plateau-like curve in the central region $|z/d| \leq 0.5$, suggesting that the heat transfer in the jet stagnation region is lowered as the rib is present.



(a) in the absence of rib



(b) in the presence of rib

Figure 14 Heat transfer contour at the velocity ratio $R = 2.8$ ($Re_j = 40,000$) for (a) in the absence of rib; (b) in the presence of rib

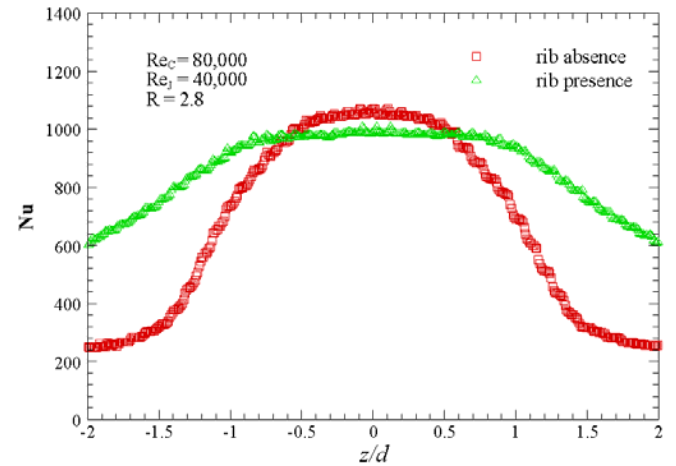


Figure 15 Spanwise variation of Nusselt number across the stagnation point at $R = 2.8$

Figure 16 shows the area-averaged Nu over the scanned area for the results presented in Figs. 8-9, 12, and 14 plotted against the velocity ratio. At the lower velocity ratio $R = 1.4$, the

presence of rib enhances the overall heat transfer; while with the increase of the velocity ratio, the enhancement effect is less obvious. At the high velocity ratio $R = 2.8$, there is nearly no perceptible difference in the area-averaged Nu between the rib-absence and rib-presence cases, respectively. However, if our attention is paid to the heat transfer uniformity instead of enhancement, it is found that the local heat transfer deteriorates in the rib corner region at lower velocity ratios $R = 1.4$. At higher velocity ratios, especially at $R = 2.8$, even though the presence of rib does not enhance the overall heat transfer significantly, the uniformity of heat transfer rate is increased.

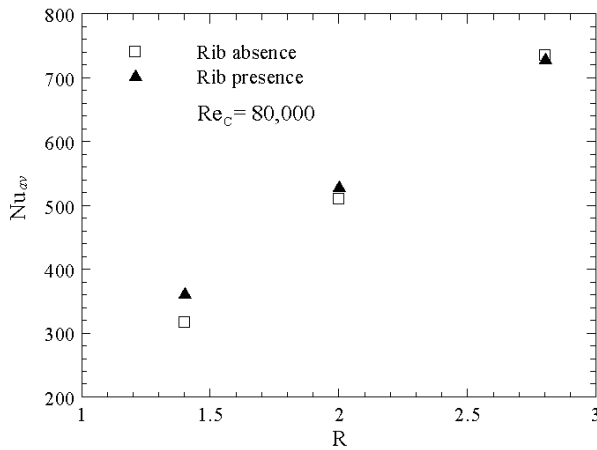


Figure 16 Area-averaged Nu over versus the velocity ratio

CONCLUSIONS

Experimental studies are carried out to investigate the effects of shallow-angle jet impingement heat transfer in crossflow with and without the presence of rib. Since the reattachment point caused by the rib due to the flow separation is coincident with the stagnation point of the impinging jet, the rib can be used to control the heat transfer characteristics of jet impingement. Liquid crystal technique is employed to measure the wall temperature and map the heat transfer coefficient distribution. For all the cases tested, it is found that the rib can effectively modify the heat transfer, especially in the stagnation region. The bell-shaped profile which is characterized by the jet impingement heat transfer is replaced by the plateau-like profile when the rib is introduced. Further inspection shows that the heat transfer enhancement is more obvious at the lower velocity ratio. However, the Nusselt number is deteriorated in the region just downstream of the rib where the fluid velocity is quite low, which will potentially cause the hot spot and jeopardize the operational safety of the heat transfer devices. At higher velocity ratio, especially at $R = 2.8$, the presence of rib makes the heat transfer rate more uniform, but meanwhile, it is found that the impinging jet effect tends to be weaker.

NOMENCLATURE

d = inner diameter of the jet tube

e = rib height

D_h = hydraulic diameter of the channel

h = heat transfer coefficient

H = height of the channel

k = thermal conductivity of air

Nu = Nusselt number = hD_h/k

Nu_0 = smooth channel Nusselt number

Nu_{av} = area-averaged Nusselt number

\dot{q}_w = heat flux on the wall

R = jet-to-crossflow velocity ratio = $R = U_j/U_0$

Re_C = crossflow Reynolds number = U_0D_h/ν

Re_J = jet Reynolds number = U_jd/ν

T_{in} = inlet temperature of air

T_w = wall temperature

U_0 = bulk velocity in channel

U_j = jet exit velocity

W = width of the channel

x = streamwise direction

y = wall-normal direction

z = spanwise direction

ACKNOWLEDGMENTS

The current research is financially supported by the Swedish research program TURBO POWER, Swedish Research Council (VR), and the Swedish National Energy Agency (STEM), which are gratefully acknowledged.

REFERENCES

1. Bouchez, J. P., and Goldstein, R. J., 1975, Impingement cooling from a circular jet in a cross flow, *Int. J. Heat Mass Transfer*, **18**, 719-730.
2. Goldstein, R. J., and Behbahani, A. I., 1982, Impingement of a circular jet with and without cross flow, *Int. J. Heat Mass Transfer*, **25**, 1377-1382.
3. Al-Sanea, S., 1992, A numerical study of the flow and heat transfer characteristics of an impinging laminar slot-jet including crossflow effects, *Int. J. Heat Mass Transfer*, **35**, 2501-2513.

4. Aldabbagh, L. B. Y., Sezai, I., and Mohamad, A. A., 2003, Three-dimensional investigation of a laminar impinging square jet interaction with crossflow, *ASME J. Heat Transfer*, **125**, 243-249.
5. Yang, Y. T., and Wang, Y. X., 2005, Three-dimensional simulation of an inclined jet with crossflow, *Int. J. Heat Mass Transfer*, **48**, 4019-4027.
6. Jia, R., Rokni, M., and Sundén, B., 2001, Impingement cooling in a rib-roughened channel with cross-flow, *Int. J. Numerical Methods for Heat & Fluid Flow*, **11**, 642-662.
7. Kanokjaruvijit, K., and Martinez-botas, R. F., 2005, Jet impingement on a dimpled surface with different crossflow schemes, *Int. J. Heat Mass Transfer*, **48**, 161-170.
8. Nam Y. W., Rhee, D. H., and Cho, J. H., 2003, Heat transfer in impingement/effusion cooling system with rib turbulators, *Proceeding of the International Gas Turbine Congress*, Tokyo, November 2-7.
9. Yan, X., Saniei, N., 1997, Heat transfer from an obliquely impinging circular air jet to a flat plate, *Int. J. Heat Fluid Flow*, **18**, 591-599.
10. Moffat, R. J., 1988. Describing the uncertainty in experimental results, *Exp. Thermal Fluid Sci.* **1**, 3-17.
11. Wang, L., and Sundén, B., 2005, Experimental investigation of local heat transfer in a square duct with continuous and truncated ribs, *Exp. Heat Transfer*, **18**, 179-197.
12. Kukreja, R. T., Lau, S. C., McMillin, R. D., 1993, Local heat/mass transfer distribution in a square channel with full and V-shaped ribs, *Int. J. Heat Mass Transfer*, **36**, 2013-2020.